Ion sound instability driven by the ion flows.

O. Koshkarov,[1, a)] A. I. Smolyakov,[1, 2] I. D. Kaganovich,[3] and V. I. Ilgisonis[2]

[1)] *Department of Physics and Engineering Physics, University of Saskatchewan 116 Science Place, Saskatoon, SK S7N 5E2, Canada*

[2)] *National Research Centre (NRC "Kurchatov Institute"), Moscow, Russia*

[3)] *Princeton Plasma Physics Laboratory, Princeton, New Jersey, 08543, USA*

Ion sound instabilities driven by the ion flow in a system of a finite length are considered by analytical and numerical methods. The ion sound waves are modified by the presence of stationary ion flow resulting in negative and positive energy modes. The instability develops due to coupling of negative and positive energy modes mediated by reflections from the boundary. It is shown that the wave dispersion due to deviation from quasineutrality is crucial for the stability. In finite length system, the dispersion is characterized by the length of the system measured in units of the Debye length. The instability is studied analytically and the results are compared with direct, initial value numerical simulations.

[a)] Electronic mail: koshkarov.alexandr@usask.ca

I. INTRODUCTION

Many natural settings of space and laboratory plasmas often include equilibrium flows of ions and/or electrons. Such situations occurs in various plasma devices for electric propulsion, plasma diodes, plasma accelerators, plasma processing devices, and emissive probe diagnostics. Plasmas permeated by energetic beams is also typical situations in space and astrophysics[1]. Such plasmas represent a typical example of a non-equilibrium system prone to instabilities due to presence of free energy reservoir from stationary flows. One of the simplest examples is the excitation of ion-sound waves when the relative velocity between electrons and ions exceeds the ion sound velocity, $v_0 > c_s$.[2–4]. In infinite plasma, the instability may occur as a result of the kinetic interaction of electrons with the ion beam (two-stream instability due to inverse Landau damping). On other hand, a number of practical plasma configurations have the finite length and it is of interest to investigate the modification/new regimes of instabilities related to the presence of boundaries. Instabilities due to accelerated ion flows are of interest for the sheath region of the plasma-material boundaries[5], plasma diodes[6,7], double layers[8–11], and electric propulsion systems[12]. In an infinite plasma, the stationary ion flow v_0 results in the Doppler shift of the ion sound waves frequency, $\omega \to \omega - kv_0$. It is shown in our paper that in a finite length systems, the ion sound waves can be destabilized due to reflections from the boundaries and coupling with ballistic modes, $\omega = kv_0$, supported by the ion flow. This instability is different from the above noted two-stream type ion sound instability where the kinetic resonances is important.

The Pierce plasma diode[13] is a well studied case of the instability driven by electron flow in a a finite length system. Various extensions of the instabilities in Pierce-like plasma systems and related numerical and experimental studies have been discussed in the literature[6,14–18]. It is shown in our paper that the problem of the ion sound waves in a system with boundaries, in a special limit of strong dispersion, is formally reduced to the Pierce like equations.

In our model we consider only fluid (hydrodynamic) effects, ions are assumed to be cold (to avoid Landau damping) and have an uniform velocity with respect to the electron component. Electrons are assumed to be in Boltzmann equilibrium (electron inertia effects are neglected). We employ analytical and numerical methods to analyze the structure of unstable eigen-modes, determine the dispersion relations and conditions for the instability, and find the frequencies and growth rates of the unstable modes.

II. OVERVIEW OF BASIC EQUATIONS AND INSTABILITY MECHANISM

In this section we present basic equations describing the ion sound waves in a finite length system and give an overview of the instability mechanism. The dynamics of cold ions is described by linearized hydrodynamic equations

$$\frac{\partial n_i}{\partial t} + v_0 \frac{\partial n_i}{\partial z} + n_0 \frac{\partial v_i}{\partial z} = 0, \tag{1a}$$

$$\frac{\partial v_i}{\partial t} + v_0 \frac{\partial v_i}{\partial z} + \frac{e}{m_i} \frac{\partial \phi}{\partial z} = 0. \tag{1b}$$

The electrons are assumed to be adiabatic and follow Boltzmann relation assuming low frequency fluctuations, $\omega < kv_{Te}$,

$$n_e = \frac{n_0 e}{T_e} \phi. \tag{2}$$

The system is closed by the Poisson equation

$$\frac{\partial^2 \phi}{\partial z^2} = -4\pi e \left(n_i - n_e \right), \tag{3}$$

where n_i,n_e,ϕ are the perturbations of the ion, the electron density and the electrostatic potential respectively, n_0 - equilibrium density, e,m_i - charge and mass of ions, T_e - electron temperature, v_0 - speed of ion flow, $v_{Te}^2 = 2T_e/m_e$ - electron thermal velocity.

For the ion injection from the left boundary, the boundary conditions similar to the Pierce problem[13] are used

$$\phi(z=0) = \phi(z=L) = n_i(z=0) = v_i(z=0) = 0, \tag{4}$$

where L - length of the system. The important feature of these boundary conditions is absence of density and velocity perturbations from the emitting boundary, e.g. as in double layer devices[11] where accelerated ions are extracted from from the plasma source chamber.

Ion sound waves on the background of the equilibrium ion flow are described equations (1), (2) and (3). For infinite length system (periodic boundary conditions), Eqs. (1), (2) and (3) result in the permittivity

$$\varepsilon(\omega, k) = 1 + \frac{1}{k^2 d_e^2} - \frac{\omega_{pi}^2}{(\omega - kv_0)^2}, \tag{5}$$

where $d_e^2 = T_e/(4\pi e^2 n_0)$ is the Debye length and $\omega_{pi}^2 = 4\pi e^2 n_0/m_i$ is the ion plasma frequency, ω,k are the frequency and wave number, respectively. The wave mode energy

corresponding to (5) is

$$\mathcal{E}(\omega,k)=\omega\frac{\partial\varepsilon}{\partial\omega}|k\phi|^2=\frac{2k^2\phi^2\omega\omega_{pi}^2}{(\omega-kv_0)^3}, \tag{6}$$

It follows that the Doppler shift due to the ion flow results in negative energy perturbations for $\omega < kv_0$. Coupling of negative and positive energy modes results in reactive instabilities[19,20]. In our case, the mode coupling occurs due to boundary conditions on the left wall as illustrated in Fig. 1. In Fig. 1a and 1b traveling wave packet arrives at the left boundary and starts forming the reflected wave. Further interaction of the reflected and original waves forms an unstable mode with an increasing (in time) amplitude as is shown in Figs. 1c and 1d.

The right boundary (with impinging ion flow), where only the potential is fixed, produce very little reflection, so that the reflected wave amplitude is much smaller than that of the incident wave (note the different scale in Fig.2c). There is no instability for the reflection from such a boundary as is illustrated in Fig. 2.

In next sections we consider the analytical solution for the unstable eigen-modes, investigate the instability conditions, describe the numerical method and compare the analytical and numerical results.

III. ANALYTICAL SOLUTIONS FOR THE EIGEN-MODES

To study the linearized system (1) analytically we seek the solution in the form $\sim e^{-i\omega t}$. Then, the equations (1-3) can be reduced to a single equation in the form

$$v_0^2\phi''''-2i\omega v_0\phi'''+\left[\frac{c_s^2}{d_e^2}-\omega^2-\frac{v_0^2}{d_e^2}\right]\phi''+\frac{2i\omega v_0}{d_e^2}\phi'+\frac{\omega^2}{d_e^2}\phi=0, \tag{7}$$

where prime is a derivative with respect to z, $c_s^2=T_e/m_i$ - the ion acoustic velocity. In the limit $v_0\to 0$, for perturbations of the form $\sim e^{ikz}$, one obtains the dispersion equation for the standard ion acoustic waves

$$\omega^2=\frac{k^2c_s^2}{1+k^2d_e^2}. \tag{8}$$

General solution of (7) can be sought as a sum of the elementary solutions $\phi\sim C_ie^{\lambda_i z}$ which are subject to the boundary conditions (4). The characteristic equation for λ has the form

$$v_0^2\lambda^4-2i\omega v_0\lambda^3+\lambda^2\left[\frac{c_s^2}{d_e^2}-\omega^2-\frac{v_0^2}{d_e^2}\right]+\frac{2i\omega v_0}{d_e^2}\lambda+\frac{\omega^2}{d_e^2}=0,$$

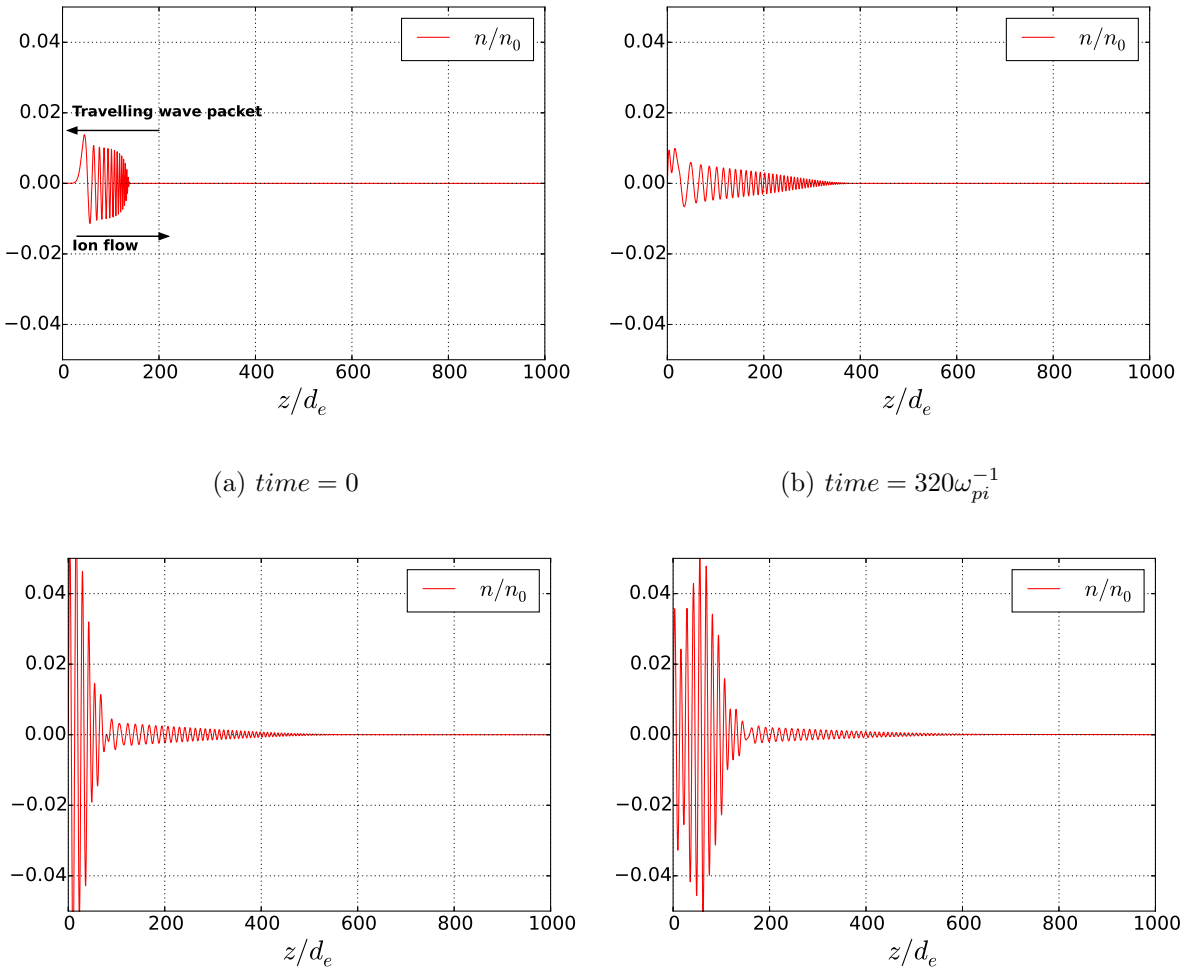

(a) $time = 0$

(b) $time = 320\omega_{pi}^{-1}$

(c) $time = 700\omega_{pi}^{-1}$

(d) $time = 1000\omega_{pi}^{-1}$

FIG. 1: Formation of unstable eigenfunction due to reflection of the wave packet from the emitting boundary on the left.

or in more convenient form

$$d_e^2\left(\lambda - \frac{i\omega}{v_0}\right)^2\left(\lambda^2 - \frac{1}{d_e^2}\right) + \frac{c_s^2}{v_0^2}\lambda^2 = 0, \tag{9}$$

which correspond to the equation (8) with Doppler shift.

A. Full quasineutrality case

The dispersion plays important role in instability mechanism. For the length scales much longer than the Debye length, the charge separation is not important and one can consider

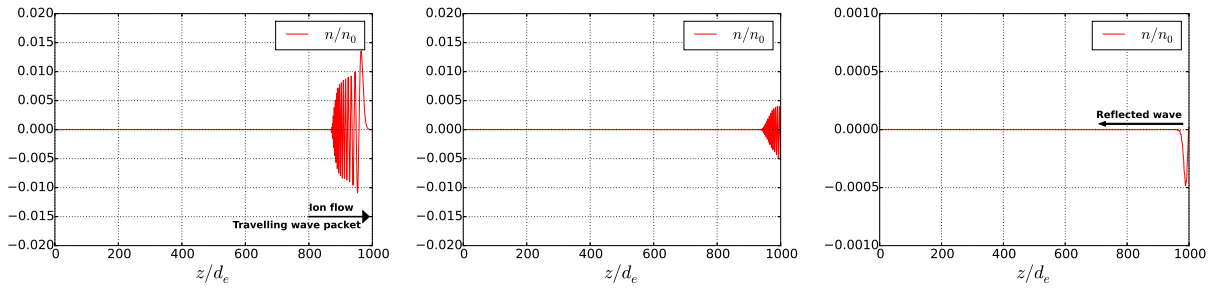

(a) $time = 0$ (b) $time = 70\omega_{pi}^{-1}$ (c) $time = 140\omega_{pi}^{-1}$

FIG. 2: Reflection from the boundary with free density and velocity perturbations (on the right).

the fully quasineutral case, $n_i = n_e$, corresponding to the absence of the dispersion.

In this limit, the solution of system (1) can be obtained in the form

$$\phi(z) = C_1 \exp\left(\frac{i\omega z}{v_0 + c_s}\right) + C_2 \exp\left(\frac{i\omega z}{v_0 - c_s}\right). \tag{10}$$

By imposing boundary conditions (4), we obtain the stable eigen-modes with the real frequencies ω

$$\omega_n = \pi n \frac{v_0^2 - c_s^2}{L c_s}, n \in \mathbb{Z}. \tag{11}$$

It is worth to note, that the formula (11) is not valid in the zero electron temperature limit, $T_e \to 0$, $c_s \to 0$, because in this case the solution for electrostatic potential will be different from (10)

$$\phi(z) = (C_1 + C_2 z) e^{\frac{i\omega}{v_0} z}, \tag{12}$$

while boundary conditions will give us the frequency

$$\omega_n = \frac{2\pi n}{L} v_0, n \in \mathbb{Z}. \tag{13}$$

Therefore, the non-dispersive waves are stable. As it will be shown below, the wave dispersion is crucial for the instability mechanism.

B. Weak dispersion case

In the long systems $d_e \ll L$, the dispersion is weak $kd_e \ll 1$, where the wave number $k \sim 1/L$. Using dispersion equation for plasma without flows (8) one gets the estimates for

the mode frequency

$$\omega \sim kc_s \text{ or } \omega \sim \frac{d_e}{L}\omega_{pi}. \tag{14}$$

We solve (9) treating Debye length as a small parameter, thus it has four roots where two of them are small $\sim O(1)$ and two of them are large $\sim O(1/d_e)$. The first pair coincide with those in quasi neutral case

$$\lambda_{1,2} = \frac{i\omega}{v_0 \pm c_s} + O(d_e^2) \sim O(1). \tag{15}$$

The second pair is

$$\lambda_{3,4} = \pm\frac{i}{v_0 d_e}\sqrt{c_s^2 - v_0^2} + \frac{i\omega c_s^2}{v_0}\frac{1}{c_s^2 - v_0^2} + O(d_e) \sim O(\frac{1}{d_e}). \tag{16}$$

Since all roots are different we can write the general solution of (7) in this form

$$\phi(z) = C_1 e^{\lambda_1 z} + C_2 e^{\lambda_2 z} + C_3 e^{\lambda_3 z} + C_4 e^{\lambda_4 z}. \tag{17}$$

The perturbed ion velocity and density from the full system (1) are found

$$4\pi e n_i = \frac{\phi}{d_e^2} - \phi'', \tag{18}$$

$$4\pi e n_0 v_i = \frac{v_0}{d_e^2}\phi + \frac{c_s^2 - v_0^2}{i\omega d_e^2}\phi' - v_0\phi'' + \frac{v_0^2}{i\omega}\phi'''. \tag{19}$$

The dispersion equation is obtained as a condition for the existence of a nontrivial solution for C_1,C_2,C_3,C_4 in the linear system of equations (4)

$$D = det\begin{pmatrix} 1 & 1 & 1 & 1 \\ e^{\lambda_1 L} & e^{\lambda_2 L} & e^{\lambda_3 L} & e^{\lambda_4 L} \\ \lambda_1^2 & \lambda_2^2 & \lambda_3^2 & \lambda_4^2 \\ \mu_1 & \mu_2 & \mu_3 & \mu_4 \end{pmatrix} = 0, \tag{20}$$

where

$$\mu_k = \left(\frac{c_s^2}{v_0^2} - 1\right)\lambda_k + d_e^2\lambda_k^3. \tag{21}$$

The dispersion equation (20) is difficult to solve analytically as there are numerous solutions on the whole complex plane. However we are interested only in those which have the largest imaginary part, since these unstable modes will dominate. The numerical solution of Eq. (20) for the long system, with the length larger than the Debye length, $L = 10d_e$, is shown in Fig. 3a. The mode frequency is consistent with estimate (14).

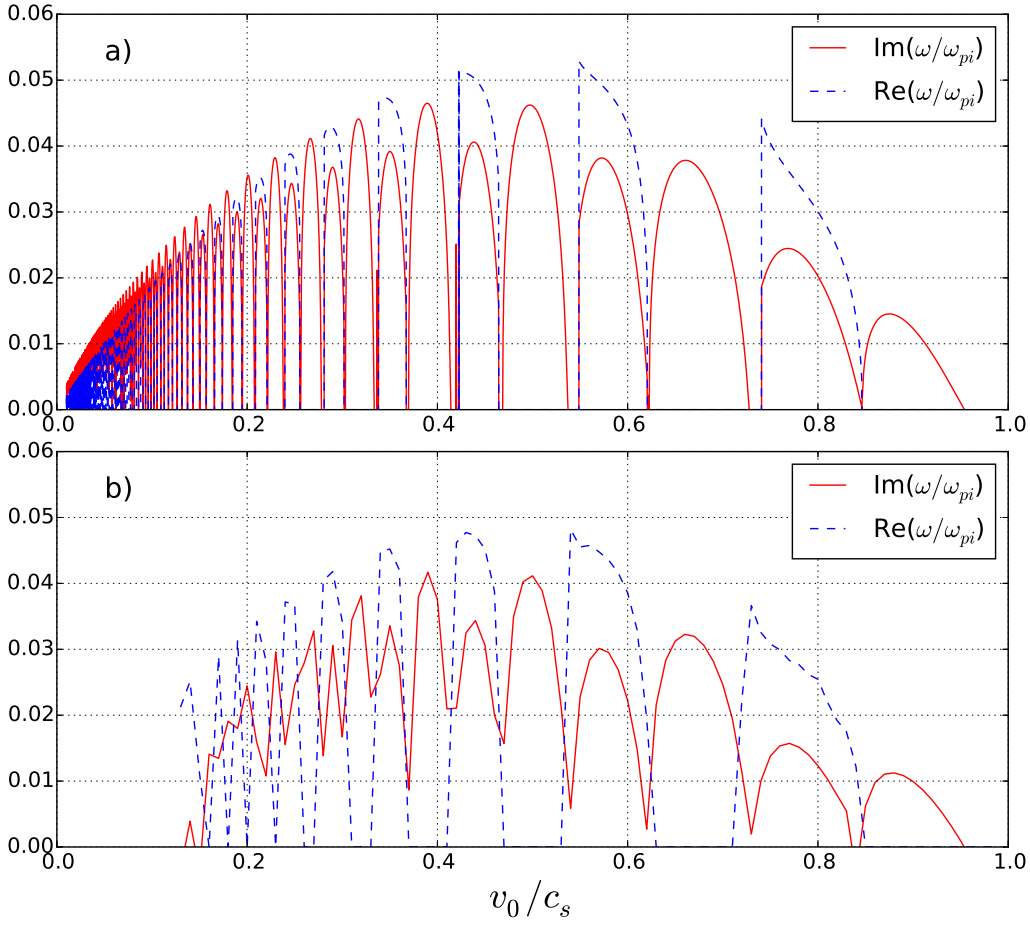

FIG. 3: The alternating zones of aperiodic ($\Re(\omega) = 0$) and oscillatory ($\Re(\omega) \neq 0$) instabilities; a) - the solution of the analytical dispersion equation (20), b) - results of numerical simulations.

For a fixed system length L, the instability growth rate depends on the dimensionless ion flow velocity v_0/c_s. The unstable regions are alternating with oscillatory ($\Re(\omega) \neq 0$) and aperiodic ($\Re(\omega) = 0$) zones. The boundaries of the zones could be found analytically using the fact that at the boundary the wave frequency is zero. Expanding (20) in Taylor series

$$D(\omega) = D(0) + \frac{\partial D(0)}{\partial \omega}\omega + O(\omega^2) = 0, \tag{22}$$

and using that $D(0) \equiv 0$, $\frac{\partial D(0)}{\partial \omega} = 0$ one finds

$$\frac{v_0^2}{c_s^2} = \frac{1}{1 + \pi^2 n^2 \frac{d_e^2}{L^2}} \text{ where } n = 1, 2, 3.... \tag{23}$$

solutions to this equation (23) correspond to zones boundaries in Fig. 3.

C. Strong dispersion case

In the short wavelength limit ($kd_e \gg 1$ or $d_e \gg L$), the dispersion modifies the solution. In this limit, the ion sound modes are reduced to the oscillations with the frequency of the order of $\omega \sim \omega_{pi}$. In this case, the reciprocal of the Debye length ($1/d_e$) is considered as a small parameter. Then the roots of the Eq. (9) are

$$\lambda_{1,2} = 0 \text{ and } \lambda_{3,4} = i\frac{\omega \pm \omega_{pi}}{v_0}, \tag{24}$$

and the general solution

$$\phi(z) = C_1 \exp\left(i\frac{\omega + \omega_{pi}}{v_0}z\right) + C_2 \exp\left(i\frac{\omega - \omega_{pi}}{v_0}z\right) + C_3 z + C_4. \tag{25}$$

This situation becomes mathematically equivalent to the Pierce instability. Imposing boundary conditions (4), one obtains an homogeneous linear system, which has nontrivial solutions when the following dispersion equation is satisfied

$$2\xi\alpha(1 - e^{i\xi}cos\alpha) + i(\xi^2 + \alpha^2)sin\alpha e^{i\xi} + i\frac{\xi^2}{\alpha}(\xi^2 - \alpha^2) = 0, \tag{26}$$

where $\xi = L\omega/v_0$ and $\alpha = L\omega_p/v_0$.
It was shown[13,21], that the dispersion equation (26) has following stability properties

$$\alpha < \pi \qquad \text{- has stable solution,} \tag{27a}$$

$$(2N-1)\pi < \alpha < 2N\pi \qquad \text{- has aperiodic instability,} \tag{27b}$$

$$2N\pi < \alpha < (2N-1)\pi \qquad \text{- has oscillatory instability,} \tag{27c}$$

where $N = 1, 2, 3....$, with a maximum growth rate $\gamma \sim v_0/L$.

There are many roots of the dispersion equation (26) on whole complex plane; as before, we choose only roots which have the largest imaginary part. The solutions which meets these criteria are shown in Fig. 4. The alternating aperiodic and oscillatory instability zones exist similar to the weak dispersion case. Fig. 3 also shows the results of direct initial value simulations described in the next section.

IV. NUMERICAL SOLUTION

To confirm our analytical results we solve the system (1) numerically. These equations have different structure and we employ the following strategy. The first two equations of

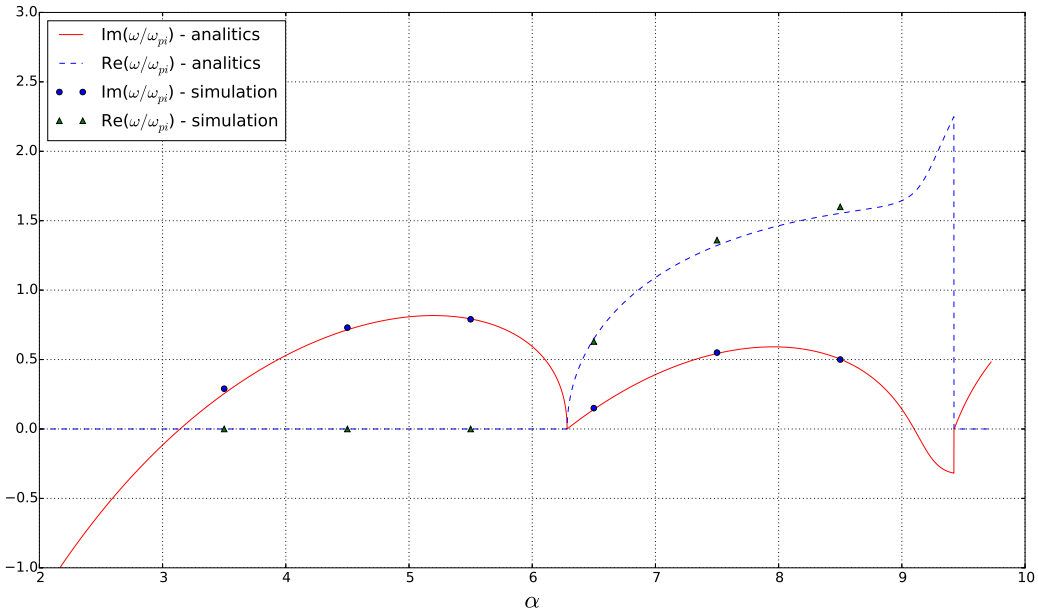

FIG. 4: The oscillatory ($\Re(\omega) \neq 0$) and aperiodic ($\Re(\omega) = 0$) instabilities in strong dispersion case. The analytical solution of (26) and numerical simulations for $L = 0.1d_e$.

(1) are considered as an explicit initial value problem (IVP), and the the third and fourth equations of (1) are solved as a boundary value problem (BVP). These subsystems are solved numerically in time and to obtain the time dependent evolution of IVP and BVP they are solved iteratively. The Poisson equation in BVP is solved at the beginning of each time step. The BVP system uses the given ion density profile (either from the initial condition or from previous time step) to produce the electrostatic potential profile. The known potential distribution allows us to solve IVP in time. As the final step, we update, the ion density and velocity profiles obtained from IVP.

Common ways to solve a BVP[22] are a family of shooting methods and finite difference schemes. We use shooting methods due to their simplicity. We have selected multiple shooting method (MSM)[23] because it is easy to parallelize, it has no disadvantages of simple shooting methods (e.g., limitations on a system length).

Our IVP is a system of hyperbolic partial differential equations (PDEs), which can be expressed in a conservative form, because of the nature of the continuity and Euler equations, which are conservative. This suggests to treat our system with a class of finite volume methods[24]. The simplest finite volume method is an upwind scheme, however we cannot use this scheme for all situation because our physical model contains the waves propagating

in opposite directions that will make the upwind unconditionally unstable. Therefore, we have resorted to Harten, Lax, Van Leer (HLL)[25] belonging to the Godunov family methods. Such schemes can be characterized by the solution of Riemann problem on computational cells. There are two types of Godunov methods: approximate and exact Riemann solvers. We used one of the kind of approximate Riemann solves - the HLL method.

For convenience all further results will be expressed in dimensionless units

$$\frac{n}{n_0} \to n, \quad \frac{z}{d_e} \to z, \quad \frac{e\phi}{T_e} \to \phi, \quad t\omega_{pi} \to t, \quad \frac{v}{c_s} \to v, \quad \frac{L}{d_e} \to L, \quad \frac{v_0}{c_s} \to v_0. \tag{28}$$

The results of numerical simulations are compared with analytical results for week and strong dispersion cases. We start our simulations with initial conditions of a uniformly distributed random noise and observe the evolution of the following quantities

$$N^2 = \int_0^L n^2(z)dz, \ \Phi^2 = \int_0^L \phi^2(z)dz, \ V^2 = \int_0^L v^2(z)dz. \tag{29}$$

Depending on the value of input parameters (L, v_0) damped (stable) or growing (unstable) solutions were observed. Unstable solution were fitted to the following curves

$$N^2, V^2, \Phi^2 \sim \cos(2\Re(\omega)t + \theta)e^{2\gamma t}, \tag{30}$$

to determine the real frequency and growth rate.

When the length of the system exceeds the Debye length ($L \sim 10d_e$), the week dispersion results are recovered. Example of frequency and growth rate dependence as a function of the ion flow velocity v_0 are shown in Figs. 3b and 5. These graphs are similar to the analytical results shown in Fig. 3a. In fact, the difference of the analytical and numerical results are of the order of the magnitude of the small parameter of the analytical theory (d_e/L). Due to the increasing density of the instability zones, very high resolution is required to recover the singular part ($v_0 \to 0$) of the analytical solution.

From the theory we know that instability will not occur in quasi-neutral case. In other words, charge separation is crucial for the instability to occur. Because in the long system charge separation is less prominent we can expect decreasing of instability growth rate with system length. This is confirmed by simulations for $L = 5$ (Fig. 5) and $L = 10$ (Fig. 3).

In the regime, when the length of the system is much smaller than the Debye length ($L \sim 0.1d_e$) the difference between analytical solution of strong dispersion approximation and numerical solution was less than few percent. This comparison is shown in Fig. 4.

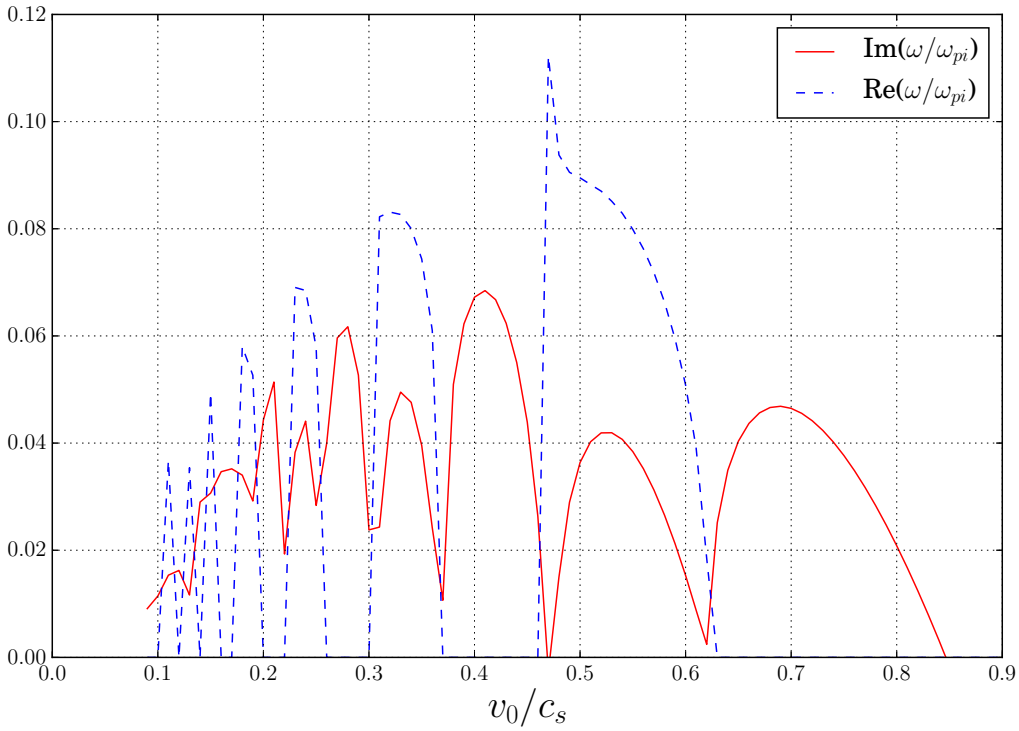

FIG. 5: Alternating oscillatory ($\Re(\omega) \neq 0$) and aperiodic ($\Re(\omega) = 0$) instabilities zones in the intermediate system length $L = 5$; numerical simulations results.

The number of zeros of unstable spatial eigenfunctions of density, velocity and electrostatic potential correlates with the zone number (27) and is defined by the value of the α parameter. In more general case, the stability of the system is governed by two parameters (v_0, L). However in general case the number of zeros correlates with a number of zone as well, examples of eigenfunctions are shown on Fig. 6.

In aperiodic zones (where real part of frequency is zero) the number of nodes does not change during the time evolution. In oscillatory zones, some nodes disappear at later times as shown in Fig. 7.

In weakly dispersive case ($kd_e \ll 1$), the addition of the Doppler shift due to the ion flow velocity results in the main order modification for the propagating modes velocities

$$v_{1,2} = v_0 \pm c_s, \tag{31}$$

which correspond the one pair of the of the roots of Eq. (9). Two other roots describe the slow dispersion effects. We have chosen very long system ($L = 1000 d_e$) so the dispersion is weak and two wave packets are well separated. Gaussian function localized in the middle

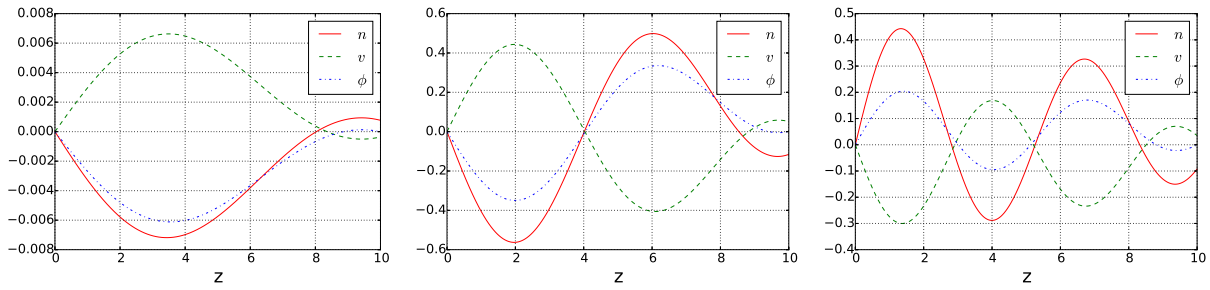

(a) zone #1 $v_0 = 0.9$ (b) zone #2 $v_0 = 0.78$ (c) zone #3 $v_0 = 0.65$

FIG. 6: Unstable spatial eigenfunctions of density, velocity and electrostatic potential for $L = 10$, for different instability zones from Fig. 3. Zone numbers in Fig. 3 are counted from the right, with the right outermost aperiodic zone as #1.

of the system was chosen as an initial condition, Fig. 8a. Fig. 8b shows that the Gaussian peak separated into two wave packets moving in opposite directions with velocities $v_{1,2}$ from Eq. (31). The right wave packet meets the wall at the right and passes through the wall with almost no reflection, as shown in Figs. 8c and 8d. Instability occurs when the slow wave packet meets the left wall (with Dirichlet boundary conditions for all variables) and is reflected, Fig. 8e. At a later time, the reflected wave and dispersion tail overlap forming an unstable eigenfunction, Fig 8e.

In strong dispersion case the equation (8) implies that oscillations with the ion plasma frequency will occur. The short system was chosen ($L = 0.1d_e$) to demonstrate this regime. Initial condition was chosen in the form of the Gaussian function localized in the middle. The evolution is shown in Figs. 9. First frame is an initial Gaussian peak which travels with velocity of the ion flow (v_0); at the same time another peak arises from the left border and starts to travel with same velocity. Note that in case of strong dispersion, the ions sound phase velocity is much reduced, $\omega/k < c_s$. When the initial Gaussian peak meets the right boundary (which has no boundary conditions except the one for electrostatic potential) it passes through, while another peak starts to transform to unstable eigenfunction at the left boundary.

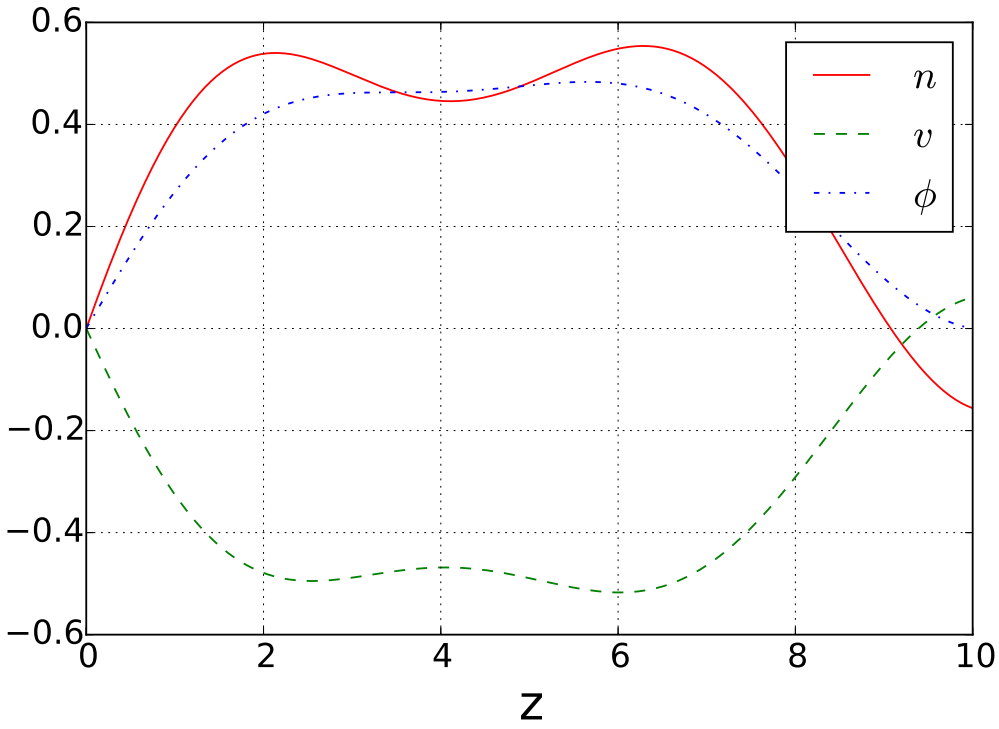

FIG. 7: Unstable eigenfunctions of density, velocity and electrostatic potential in the oscillatory zone #2 $v_0 = 0.78$, $L = 10$, at a later time.

V. CONCLUSION

We have investigated the ion acoustic instability induced by the ion flow in a finite length system; the situation which is relevant to various plasma devices such as electric propulsion and emissive probe diagnostics. It was shown that the length of the system measured in units of the Debye length and ion flow velocity measured in units of the ion acoustic velocity are important parameters which control the instability.

For long systems ($d_e \ll L$) the analytical dispersion equation was obtained describing the aperiodic and oscillatory instability zones. The boundaries of the instabilities are defined by the condition (23). The instability criteria could also be written in the form

$$\frac{1}{1+\pi^2\frac{d_e^2}{L^2}} > \frac{v_0^2}{c_s^2}. \tag{32}$$

For short systems ($d_e \gg L$) the dispersion equation was obtained in the form equivalent to the Pierce dispersion equation. In this case, the following instability criteria has been

obtained

$$L\omega_{pi}/\pi > v_0. \tag{33}$$

Analytical theory was confirmed by the results of direct initial value numerical simulations. We have investigated the structure of the eigenfunctions in the unstable zones. It is shown that the order of the instability zone correlates with a number of nodes in the corresponding eigenfunction. Our numerical simulations show that the instability occurs as a result of the mode coupling mediated by the boundaries.

The instability mechanism in a finite length system is different from the kinetic ion sound instability[26] in infinite plasmas. The dispersion equation for the latter can be written in the form

$$1 + \frac{\omega_{pi}^2}{k^2 c_s^2} - \frac{\omega_{pi}^2}{\omega - kv_0} + i\sqrt{\frac{\pi}{2}\frac{m_e}{m_i}}\frac{\omega_{pi}^2 \omega}{k^3 c_s^3} = 0. \tag{34}$$

Treating $\epsilon = \sqrt{\frac{\pi}{2}\frac{m_e}{m_i}}$ as a small parameter, one obtains the growth rate

$$\gamma = \frac{\epsilon k c_s}{2(1+k^2 d_e^2)^2}\left(-1 \pm \frac{v_0}{c_s}\sqrt{1+k^2 d_e^2}\right). \tag{35}$$

The instability condition has a form

$$\frac{1}{1+k^2 d_e^2} < \frac{v_0^2}{c_s^2}, \tag{36}$$

which is complementary to the condition (32).

The excitation of large scale perturbation and soliton formation was observed in a number of experiments[27,28]. Similar structures may be excited by ion flow due to the mechanism identified in our paper which is operative in systems of a finite length and in situations when the ion flow velocity is below the ion acoustic speed. The excitation of ion sound waves in a finite length system was observed in numerical particle-in-cell simulations with emissive walls[29,30]. The mechanism described in this paper can also be relevant to the instabilities observed in double layer experiments[10,31,32].

Acknowledgments

This work was supported in part by NSERC of Canada and US Air Force Office of Scientific Research.

REFERENCES

[1] J. Vranjes. New features of ion acoustic waves in inhomogeneous and permeating plasmas. *Astronomy & Astrophysics*, 554:A90, 2013.

[2] A. A. Galeev and R. Z. Sagdeev. Nonlinear plasma theory. In M.A. Leontovich, editor, *Reviews of Plasma Physics*, volume 7. Consultants Bureau, New York, 1979.

[3] F. Skiff, G. Bachet, and F. Doveil. Ion dynamics in nonlinear electrostatic structures. *Physics of Plasmas*, 8(7):3139–3142, 2001.

[4] J. A. Wesson, A. Sykes, and H. R. Lewis. Ion-sound instability. *Plasma Physics*, 15(1):49, 1973.

[5] R. T. Farouki, M. Dalvie, and L. F. Pavarino. Boundary-condition refinement of the Child-Langmuir law for collisionless dc plasma sheaths. *Journal of Applied Physics*, 68(12):6106–6116, 1990.

[6] A. Y. Ender, H. Kolinsky, V. I. Kuznetsov, and H. Schamel. Collective diode dynamics: an analytical approach. *Physics Reports*, 328(1):1 – 72, 2000.

[7] H. Schamel and S. Bujarbarua. Lagrangian description of ion dynamical effects in plasma diodes. *Physics of Fluids B: Plasma Physics*, 5(7):2278–2285, 1993.

[8] A. M. Keesee, E. E. Scime, C. Charles, A. Meige, and R. Boswell. The ion velocity distribution function in a current-free double layer. *Physics of Plasmas*, 12(9):093502, 2005.

[9] S. D. Baalrud and C. C. Hegna. Kinetic theory of the presheath and the Bohm criterion. *Plasma Sources Science & Technology*, 20(2):025013, 2011.

[10] C. Charles. A review of recent laboratory double layer experiments. *Plasma Sources Science and Technology*, 16(4):R1, 2007.

[11] J. C. Johnson, R. L. Merlino, and N. d'Angelo. Double layers formed by ion-beam injection in a double-plasma device. *Journal of Physics D: Applied Physics*, 22(10):1456, 1989.

[12] A. Kapulkin and E. Behar. Ion Beam Instability in Hall Thrusters. *IEEE Transactions on Plasma Science*, 43(1, 1):64–71, 2015.

[13] J. R. Pierce. Limiting stable current in electron beams in the presence of ions. *Journal of Applied Physics*, 15(10):721–726, 1944.

[14] J. R. Cary and D. S. Lemons. Unstable oscillatory Pierce modes of neutralized electron beams. *Journal of Applied Physics*, 53(4):3303–3304, 1982.

[15]S. Kuhn. The physics of bounded plasma systems (BPS's): Simulation and interpretation. *Contributions to Plasma Physics*, 34(4):495–538, 1994.

[16]T. L. Crystal and S. Kuhn. Particle simulations of the low$-\alpha$ Pierce diode. *Physics of Fluids*, 28(7):2116–2124, 1985.

[17]B. B. Godfrey. Oscillatory nonlinear electron flow in a Pierce diode. *Physics of Fluids*, 30(5):1553–1560, 1987.

[18]M. Hiroshi, H. Yokoyama, and D. Summers. Computer simulations of the chaotic dynamics of the Pierce beam-plasma system. *Physics of Plasmas*, 3(1):177–191, 1996.

[19]C. N. Lashmore-Davies. Negative energy waves. *Journal of Plasma Physics*, 71:101–109, 4 2005.

[20]M. V. Nezlin. *Physics of Intense Beams in Plasmas*. IOP Publishing, Bristol and Philadelphia, 1993.

[21]A. B. Mikhailovskii. *Theory of plasma instabilities*. Atomizdat, Moscow, 1975.

[22]W. H. Press, S. A. Teukolsky, W. T. Vetterling, and B. P. Flannery. *Numerical Recipes: The Art of Scientific Computing*. Cambridge University Press, New York, NY, USA, 3 edition, 2007.

[23]U. M. Ascher and S. Y. P. Chan. On parallel methods for boundary value ODEs. *Computing*, 46(1):1–17, 1991.

[24]R. J. LeVeque. *Finite Volume Methods for Hyperbolic Problems*. Cambridge University Press, Cambridge, New York, 2002.

[25]P. L. Roe. Approximate Riemann solvers, parameter vectors, and difference schemes. *Journal of Computational Physics*, 43(2):357 – 372, 1981.

[26]A. I. Akhiezer. *Plasma electrodynamics*. Pergamon Press, Oxford, 1975.

[27]K. E. Lonngren. Soliton experiments in plasmas. *Plasma Physics*, 25(9):943, 1983.

[28]A. Hirose, O. Ishihara, S. Watanabe, and H. Tanaca. Response of ion acoustic waves to an impulse. *Plasma Physics*, 20(11):1179, 1978.

[29]J. P. Sheehan, N. Hershkowitz, I. D. Kaganovich, H. H. Wang, Y. Raitses, E. V. Barnat, B. R. Weatherford, and D. Sydorenko. Kinetic theory of plasma sheaths surrounding electron-emitting surfaces. *Phys. Rev. Lett.*, 111:075002, Aug 2013.

[30]D. Sydorenko. *Private Communication*, 2014.

[31]C. Rapson, O. Grulke, K. Matyash, and T. Klinger. The effect of boundaries on the ion acoustic beam-plasma instability in experiment and simulation. *Physics of Plasmas*

(1994-present), 21(5):052103, 2014.

[32]A. Aanesland, C. Charles, M. A. Lieberman, and R. W. Boswell. Upstream ionization instability associated with a current-free double layer. *Phys. Rev. Lett.*, 97:075003, Aug 2006.

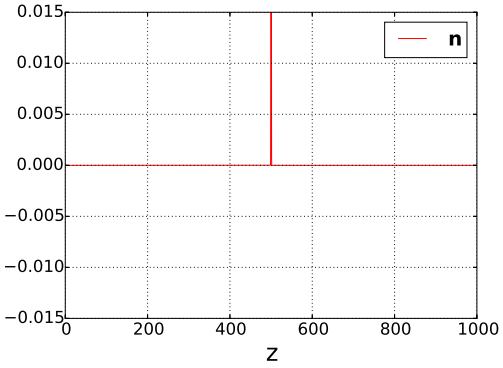

(a) t = 0

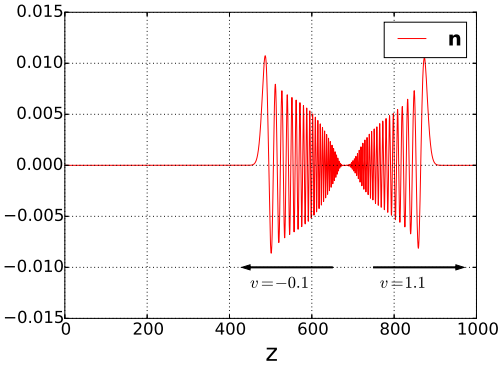

(b) t = 200

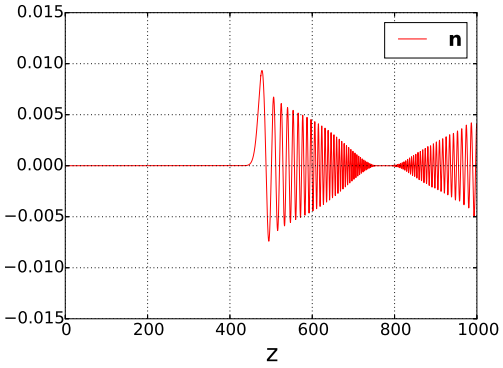

(c) t = 300

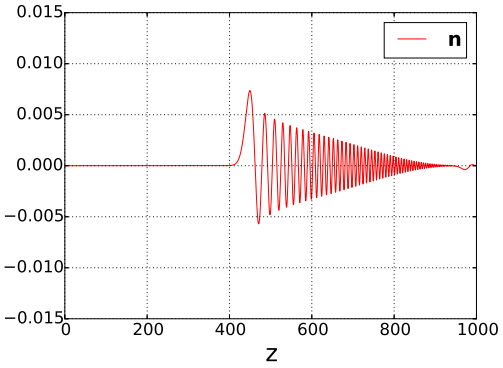

(d) t = 600

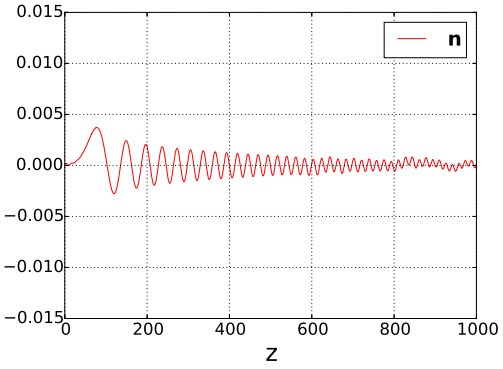

(e) t = 4400

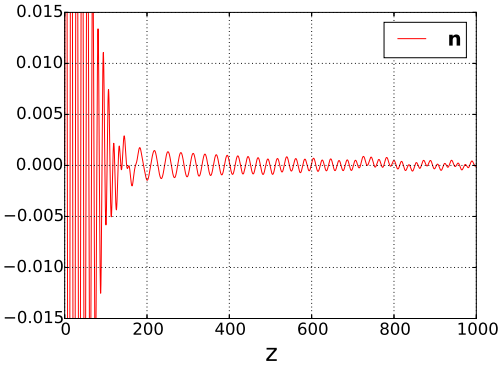

(f) t = 5100

FIG. 8: Evolution of the initial Gaussian pulse in the weak dispersion case: (a) - initial condition; (b) - initial perturbation splits into two traveling wave packets, the one traveling to the right with $v_0 + c_s = 1.9$ and the one traveling to the left with $v_0 - c_s = -0.1$; (c) - the right wave packet is passing through the right wall barely reflecting; (d) - the beginning of the reflection of the left wave packet from the wall and forming of the unstable eigen-function.

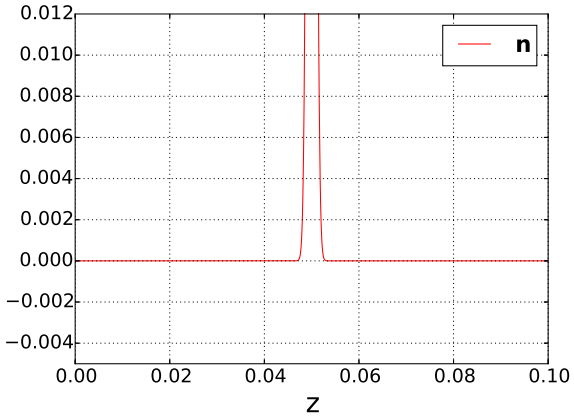

(a) t = 0

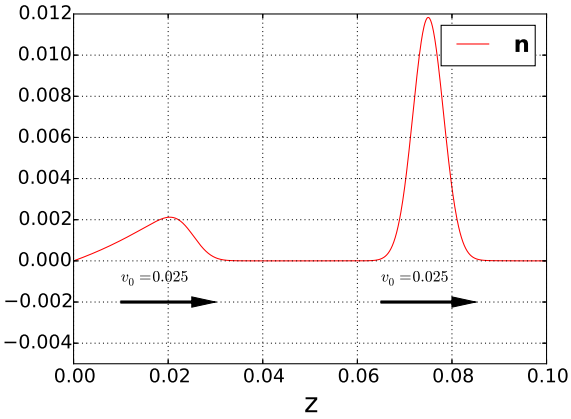

(b) t = 100

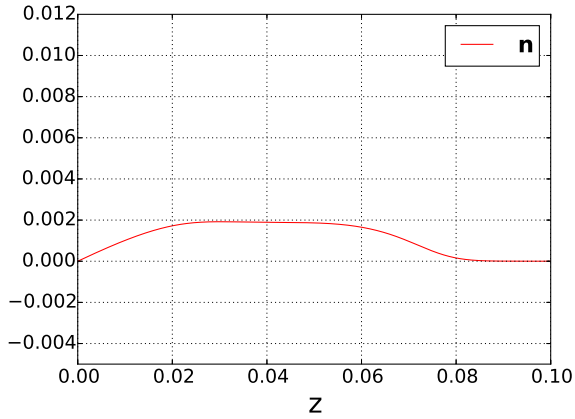

(c) t = 300

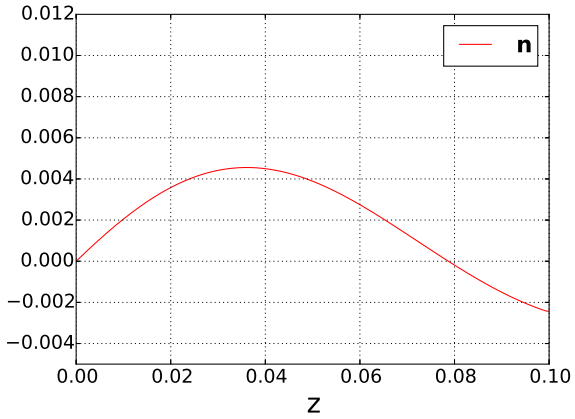

(d) t = 900

FIG. 9: Dynamics in the strong dispersion case: (a) - initial state; (b) - the initial Gauss pulse travels with velocity $v_0 = 0.025$ to the right, another pulse start to grow and travels to the right with the same velocity; (c) - the initial pulse approaches the left boundary and the unstable eigen-function forms.